Astron. Astrophys. 329, 265–275 (1998)

ASTRONOMY
AND
ASTROPHYSICS

Velocity fields of planetary nebulae⋆

Krzysztof Gesicki[1], **Albert A. Zijlstra**[2], **Agnes Acker**[3], **and Ryszard Szczerba**[4]

[1] Torun Center for Astronomy, UMK, ul. Gagarina 11, PL-87100 Torun, Poland (gesicki@astri.uni.torun.pl)
[2] European Southern Observatory, Karl Schwarzschild Strasse 2, D-85748 Garching b. München, Germany (azijlstr@eso.org)
[3] Observatoire de Strasbourg, 11, rue de l'université, F-67000 Strasbourg, France (acker@astro.u-strasbg.fr)
[4] Nicolaus Copernicus Astronomical Center ul. Rabianska 8, PL-87100 Torun, Poland (szczerba@ncac.torun.pl)

Received 28 February 1997 / Accepted 8 August 1997

Abstract. Density distributions and velocity fields are derived for four spatially resolved planetary nebulae, based on high-resolution long-slit emission line spectra. We use a photo-ionization code to fit the spectra and to derive the nebular structure, assuming spherical symmetry. We present the results for individual nebulae and compare with three objects analyzed earlier. The expansion velocities are found to increase outward: this is shown to be likely related to the presence of an ionization front. Six PN in the sample are found to be ionization bounded. For one object, which has a WR-type central star, a large amount of turbulence or irregular structure in the velocity field is found. The results are in agreement with hydrodynamical calculations, in which the velocities also tend to increase with distance from the star. However, the common presence of an ionization front was not predicted.

Key words: planetary nebulae: general – planetary nebulae: individual: M 3-12, NGC 6620, M 3-15, M 1-40

1. Introduction

The most important parameter describing the dynamics of a planetary nebula is its expansion velocity. Expansion velocities can be derived from measurements of the line splitting or of the full widths at half maximum (FWHM) of an emission line (see e.g. the catalogue published in Weinberger 1989). Frequently only a single value is available for a particular PN. Some papers specifically addressing the internal motions (e.g. Sabbadin et al. 1984, 1986) still use a unique expansion velocity for a specific PN: in Sabbadin et al., the "radius versus velocity" relation is only a correlation between the expansion velocity and the outer radius for different nebulae or for one nebula evolving in time.

Internal velocity fields in planetary nebulae (hereafter PN) are however not well described by simple, uniform expansion. Attempts to find the velocity distribution inside PN were first made by comparing expansion velocities measured in different ionic lines (Wilson 1950, Pottasch 1984). A velocity gradient has been suggested from this, with expansion velocity increasing outward. With the advance in observational techniques (CCD cameras and long-slit spectroscopy) more detailed analysis of nebular structures, with emphasis on complicated ones, became possible. An example is the work of Chu et al. (1991) with imagery and spectroscopic studies of NGC 6751. Several structures in this large PN could be investigated in detail, but regarding the low-order velocity field they only comment that a velocity gradient is likely.

The velocity field across a PN can be predicted from hydrodynamical calculations. Examples concerning spherical nebulae can be found in Marten & Schönberner (1991), Frank (1994), Mellema (1994), Schönberner et al. (1997). Comparisons with observations are only applied to generic nebulae. We are not aware of any publication presenting a match between a detailed hydrodynamic model and a specific PN.

In a previous paper (Gesicki et al., 1996, Paper I), we used observed emission-line profiles of PN to study the problem of velocity fields. The spectral line profile arises from a convolution of the density and velocity distribution. Using the density distribution derived from monochromatic images, information about the velocity field can be obtained. In Paper I we analyzed spectra of nebulae taken through small circular apertures centred on the PN. However, a more detailed analysis can be done when instead of an aperture spectrum a long-slit spectrum yielding spatial information along the slit is available.

In this paper we analyze four PN for which high-resolution (5×10^4) long-slit spectra are available of three diagnostic lines. In the next section we describe how the spatial information is extracted from the spectra. Retaining the assumption of spherical symmetry, we present the model analysis for the selected PN. We find the presence of positive velocity gradients in the nebulae, possibly related to the presence of ionization fronts.

Send offprint requests to: K. Gesicki

⋆ Based on observations taken at ESO

2. Calculations

The computer models are described in detail in Paper I. We present in this section a short summary of the method, focusing on the extension to spatially resolved line profiles.

For each nebula we construct a model, under the assumption that the PN can be described as a spherical shell defined by an inner and an outer radius, a radial density distribution and a radial velocity field. The outer radius is given by the observed angular diameter and the adopted distance; the inner radius is used as a free parameter, for which we usually adopt the value of 0.4 of the outer radius but in some cases it can be estimated from observations (see the discussion of NGC 6620). The stellar ionizing flux is assumed to have a black-body distribution with the effective temperature $T_{\rm eff}$ of the central star taken from observations. The luminosity of the star is derived from the observed V-band magnitude, the observed $T_{\rm eff}$ and the adopted distance. For each analyzed nebula we adopt the chemical composition from the literature.

The photoionization structure is calculated first, followed by the integrated emission-line strengths. The ionized mass is adjusted until the calculated total flux in Hβ is consistent with the observed one. The free parameters are adjusted simultaneously to obtain agreement between the predicted line ratios and plasma parameters and the observed values. Finally the calculated line profiles are compared with the observations.

In Paper I the density structure was adopted from analysis of the images, and the velocity field was adjusted in order to fit the line profiles. Note that all nebulae were significantly larger than the size of the aperture. For the nebulae modeled in the present paper no suitable monochromatic images exist in the literature, requiring us to start with an arbitrary density distribution. As a starting approximation an inverse parabolic density distribution was used. The spectral-line fitting procedure allows us later to correct this distribution.

We assume that the PN is spherical (circular when projected onto the sky), and that the slit is well centred on the nebular image. The slit is projected on the CCD pixels; each pixel along the length of the slit yields a spectrum. For the CAT/CES spectrograph the slit width used was $2''$ and the (binned) pixels were also $2''$ so that each spectrum sampled a square element on the sky. Due to seeing effects neighbouring pixels are interdependent. To take this into account we assumed for our calculations that the sampled area is larger than $2''\times2''$ and overlaps with neighbouring areas: both the slit width and the pixel size are broadened compared to the geometrical size. A schematic drawing is presented in Fig. 1. The ratio of the slit width to the nebular diameter can be estimated from the observed spatial extension along the slit, and from the fact that only if the slit is significantly narrower than the nebular angular size can the characteristic double-peaked line profile be observed. In the example of Fig. 1, $2''$ corresponds to 0.25 of the nebular diameter, so that the nebular radius corresponds to two independent $2''\times2''$ areas. Because of the slit/pixel broadening, each is enlarged to 0.5 of the diameter giving 50% overlap between the elements. We do not use data from the outermost areas where the signal may be heavily affected by seeing smearing. In Fig. 1 this corresponds to the top square.

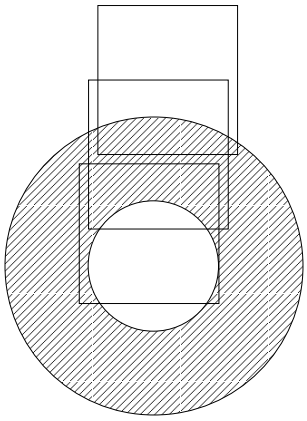

Fig. 1. Schematic presentation of modeled long-slit pieces

The line-profile variations along the slit yields the nebular angular size: angular diameters estimated in this way are listed in Table 1.

The spatial variation of the line intensity along the slit depends on the density distribution. We adjust the radial density distribution in the model until satisfactory agreement is reached. Simultaneously we vary the velocity field to fit the detailed line profiles, such as the velocity separation of the double peaked profiles and the extent of the line wings (e.g. Spyromilio 1995). The spectral resolution of the instrument as well as different seeing conditions for different sets of observations are taken into account. Remaining discrepancies can be reduced by introducing turbulent broadening of spectral lines.

As in Paper I, the fits cannot be considered unique. Following the method developed in that paper we try to find the simplest velocity and density distribution possible, described by the smallest number of parameters. In practice it is sufficient to restrict ourselves to either a constant velocity, or to a positive, smoothly varying velocity gradient. We gradually proceed from a simple to a more complex velocity field until satisfactory fits to the line profiles are obtained. It is relatively straightforward to accurately fit a single spectral line. Simultaneously fitting the three observed lines gives a much more constrained solution: each line has a different spatial emission distribution, and its shape is most sensitive to the assumed velocity near the location of its peak emission. The maxima for [O III] and [N II] are well separated in the nebula and allow us to deduce a simple velocity field in the inner and the outer regions with a smooth transition in between. The presented radial distributions were obtained by applying smoothed splines. Elaborate dependencies were not investigated, because of the limitations implied by the spectral resolution of our observations ($5\,{\rm km\,s^{-1}}$) as well as by the simplifications inherent in the model. We stop the procedure when the introduction of a change to the velocity field in a part of the nebula worsens the agreement with the observed line profiles. Such situations are presented below.

The PN described here are only marginally resolved and the additional information achieved from the long-slit data is limited. We selected PN which are thought to be near the galactic centre, for which the distances are reasonably well known. The limited spatial resolution is however not a problem for the study of the overall (low-order) velocity gradient. Better spatial resolution could have shown a wealth of detail which the model is not designed to fit, including possible non-spherical morphologies. However, better spatial resolution could have improved the determination of the nebular diameter (e.g. Bedding & Zijlstra 1994).

3. The observations

The observations were carried out with the ESO 1.4m CAT telescope in June and July 1993, and March 1994. In July, the [O III] 5007Å line was observed using the short camera in the blue arm, giving a resolution of 30000 (0.17Å or 10 km s^{-1}). In June 1993 and March 1994 the Hα line and neighbouring [N II] 6548, 6583Å lines were observed, using the long camera which gives a resolution of 60000 (0.1Å or 5 km s^{-1}). For Hα the higher resolution is partly offset by the larger thermal broadening. Integration times varied from a few to 30 minutes depending on the line flux. The slit had a width of 2″ and a length of 20″; the CCD was binned to obtain 2″ pixels, consistent with the seeing. The wavelength calibration was done with ThAr spectra, and also checked by observing well-known planetary nebulae as velocity standards. The data reduction involved flat fielding and wavelength calibration; no flux calibration was performed. The velocity scale was corrected for the Earth's motion to obtain heliocentric velocities: agreement to within 3 km s^{-1} is found between the Hα and [O III] measurements (reduced in different ways).

The CAT suffers from field rotation so that the orientation of the slit on the sky is not known. For long exposures the slit orientation may also change during an exposure, although this will be a minor effect for the present data. The [OIII] and Hα/[NII] data may have a different slit orientation. The unknown orientation is not a problem for spherically symmetric nebulae and does not affect the modeling where symmetry is assumed. However, the spectra for bipolar or elliptical nebulae will depend on the slit orientation and this will also affect comparison with images. The limited spatial resolution reduces the effect.

4. Analysis of the selected nebulae

Input parameters used in the models of the four analyzed PN are listed in Tables 1 and 2, together with a number of observational parameters for which comparison with model predictions are possible.

The angular diameter, distance, linear radius, $\log(F(\mathrm{H}\beta))$ and ionized mass are interdependent in the models. The listed values are obtained as described above. The angular diameters of the models are defined as the diameter where the surface brightness has decreased to 20% of its maximum value. The agreement between observation and calculation is not perfect but acceptable considering the observational uncertainties, asymmetries of the PN which are evident in the spectra and images, and the simplifications implicit in the model.

The most direct check of our photoionization model comes from a comparison of the line ratios as presented in Table 2. We can also compare the plasma parameters, i.e. electron temperature and density, between our photoionization model and published values estimated from selected line ratios. The values are presented in Table 1. The agreement for the electron temperatures is quite good, but significant discrepancies are found for the electron densities. Test calculations show that the value of electron density is very sensitive to the changes in the [S II] $I(\lambda 6717)/I(\lambda 6731)$ line ratio (e.g. varying this ratio from 1.0 to 0.8 increases the estimated electron density by a factor of two). The [S II] lines are usually weak and difficult to accurately measure.

The adopted $T_{\rm eff}$ and $\log\left(L/L_{\odot}\right)$ sometimes differ from values found in literature: in these cases the adopted values better explain the observed line ratios. The line ratios will also depend on the assumed chemical composition but the chemical analysis is beyond the main scope of our paper, nor do we discuss how the photoionization structure is affected by the assumption of a black-body stellar atmosphere. All the presented models are ionization bounded (where the outer nebular radius equals the ionization boundary): density-bounded nebulae do not reproduce the line ratios as well.

We define V_{av} as the radially averaged value of the expansion velocity over the shell, weighed by the density distribution:

$$V_{av} = \frac{\int_{R_i}^{R_o} 4\pi r^2 \rho(r) V(r) dr}{\int_{R_i}^{R_o} 4\pi r^2 \rho(r) dr}$$

It mainly represents the area of higher density, but takes into account the increase of the expansion velocity in the lower-density outer regions, which we require to explain the shape of the line wings. It does not include turbulent motions which can broaden the spectral lines. The value of V_{av} is larger than the expansion velocity estimated from the separation of the double line peak, but is comparable to the velocity estimated from the FWHM of the lines. All the definitions for the expansion velocity are presented in Table 1.

In Figs. 2-5 we compare the observed line shapes with the models. The left set of three diagrams present the line profiles integrated over the slit, where the circles indicate the observations and the solid line gives the model. The diagrams on the right show the variation along the slit: the data shows both sides of the centre but the calculated profiles are plotted only for half of the slit based on the assumed spherical symmetry. The observed points are marked with squares for spectra from central regions and triangles for outer spectra; open symbols correspond to one side of the long slit, and filled filled to the opposite side. If there is a single centred spectrum, as for M 3-12, it is indicated with stars. The diagrams are given for hydrogen (observed is Hα but the calculations in fact refer to Hβ), [N II] 6585Å and [O III] 5007Å. The highest intensity profiles are normalized to unity. Line profiles near the edges of the nebula (with

Table 1. Parameters adopted for the calculation

	M 3–12 PN G 5.2+5.6	NGC 6620 PN G 5.8-6.1	M 3–15 PN G 6.8+4.1	M 1–40 PN G 8.3-1.1	Ref.
distance [kpc]	8.0	8.0	4.0	2.5	CGPN
NEBULA					
Angular diameter [arc sec]					
from literature: optical or radio	6 or 7.5	8 or 5	4.2 or 5	5 or 4.3	CGPN
from model Hβ image	6.5	6	5	4.6	this work
model outer radius [pc]	0.15	0.14	0.06	0.042	
extinction c(Hβ)	1.10	0.60	2.1	2.7	TASK92
log F(Hβ)					
observed, dereddened	-11.2	-11.13	-10.35	-10.01	CGPN
calculated from model	-11.14	-11.07	-10.11	-10.14	
[O III] electron temperature [K]					
from literature	–	9900	11200	–	AK
from our models	12602	9449	9048	10260	
[N II] electron temperature [K]					
from literature	–	8800	–	9500	AKSJ
from our models	12100	9680	9700	9790	
[S II] electron density [cm^{-3}]					
from literature	1020	2470	2500*	7880	AK, AKSR, AKSJ
from our models	948	893	3805	3250	
$V_{\rm exp}$ [km s^{-1}] observed					this work
[O III] peak separation	18	16	–	–	
[O III] FWHM	26	25	19	24	
[N II] peak separation	17	21	–	21	
[N II] FWHM	28	31	19	32	
V_{av} [km/s] calculated from model	30	27	16	27	
additional turbulent broadening [km/s]	no	no	15	no	
ionized mass [$M_\odot$] calculated from model	0.57	0.45	0.19	0.067	
STAR					
magnitude V	–	19.6:	–	18.3	CGPN
spectrum description	–	–	[WC 4-6]	–	CGPN
log($T_{\rm eff}$) from literature	4.9, 4.81	5.04, 5.02	4.74	5.14, 5.07	SKAS, PAKS
log($T_{\rm eff}$) adopted	5.0	5.04	4.9	5.15	
log($L/L_\odot$) from literature	3.0, 3.8	2.9, 3.7	3.8	3.6, 4.0	SKAS, ZK
log($L/L_\odot$) adopted	3.2	3.3	3.6	3.3	

References: AK = Aller & Keyes (1987), AKSJ = Acker et al. (1989), AKSR = Acker et al. (1991), CGPN = Acker et al. (1992)
PAKS = Preite-Martinez et al. (1989), SKAS = Samland et al. (1992), TASK92 = Tylenda et al. (1992), ZK = Zhang & Kwok (1993)
* value from AK, however AKSR published value of 24330

intensity < 0.3 of that of the central profile), which may be heavily affected by seeing smearing, are not shown. The bottom three diagrams show the model density and velocity fields (left), monochromatic surface brightness profiles (centre) and the calculated electron temperature and density (right).

4.1. PN M 3-12 (PN G 5.2+5.6)

This PN is likely a member of the Galactic bulge (GCPN, Van de Steene and Zijlstra 1994). A distance of 8 kpc has therefore been assumed. The spatial extent along the slit is relatively large, corresponding to five pixels (see the right panels in Fig. 2). The model of PN has therefore a relatively large outer radius (0.15 pc) and a high value of the ionized mass. The mass would be reduced if a smaller distance and/or a smaller radius was

Table 2. Comparison of observed (dereddened) and calculated line ratios, relative to I(Hβ) = 100

	M 3-12 PN G 5.2+5.6		NGC 6620 PN G 5.8-6.1			M 3-15 PN G 6.8+4.1			M 1-40 PN G 8.3-1.1	
line	observed (1)	our model	observed (1)(2)	(3)	our model	observed (1)	(3)	our model	observed (1)(2)	our model
[Ne III] 3868	-	92	-	120	31	-	57	73	-	81
[Ne III] 3969	-	29	23	-	10	-	-	23	-	25
He II 4686	15	13	23	26	19	10	-	5	46	34
Ar IV 4740	-	2.4	3	3	6	-	-	3	13	24
[O III] 5007	584	589	1190	1292	1365	914	1026	631	1543	2005
[O I] 6300	-	2.6	9	8	12	-	-	2	13	6
[S III] 6311	-	1.4	3	2	4	-	-	8	6	3
[N II] 6584	37	53	266	225	346	46	39	86	384	289
[S II] 6717	2.1	4.1	18	19	22	2	2.1	18	9	9
[S II] 6731	2.5	4.6	28	28	26	4	4	30	18	14
Ar III 7136	15	13	27	21	26	-	13	6	38	24

(1) CGPN, Acker et al. (1992) (dereddened)
(2) Acker et al. (1989) (dereddened)
(3) Aller & Keyes (1987)
- no suitable observations available

adopted. A smaller distance could still be consistent with bulge membership, because of the large intrinsic depth of the bulge. Zijlstra et al. (1997) find indications that the Bulge PN for which high-resolution spectra exist sample primarily the near side of the Bulge.

The observed line ratios are reproduced very well (see Table 2). The assumed width of the seeing-broadened slit corresponds to 0.75 of the PN diameter (the pixels along the slit are centered on 0, 0.5 and 1 times $R/R_{\rm out}$. The fit of the line profiles presented in Fig. 2 is obtained with an expansion velocity which increases with radius, and the nebula seems to have a high density and low velocity central region surrounded by an accelerating lower density shell. The hydrogen and [O III] lines, formed in the inner layers, are reproduced very well by our model but the [N II] profile presents a worse fit. Adding turbulent motions improves the [N II] fit but worsens the other two. The [N II] line is formed in extended outer regions, as is evident in the modeled surface brightness distribution (Fig. 2), and may be broadened by a high velocity region in the outer shell, as is sometimes seen in PN (e.g. Frank et al. 1993).

4.2. PN NGC 6620 (PN G 5.8-6.1)

For this PN we also assume the distance of the galactic centre. The seeing-corrected slit width adopted for the profile calculation is 0.55 of the PN diameter (the pixels along the slit are centred on 0.25 and 0.75 times $R/R_{\rm out}$. The clear splitting of the central profiles in the [O III] line indicates a relatively large inner nebular radius. The empty cavity must be comparable in size to the central pixel of the slit: if it were much smaller the splitting would disappear. A simple density structure with an increasing velocity gradient, similar to the previous case, can explain the observed line shapes (see Fig. 3) as well as the line ratios (Table 2).

4.3. Nebula M 3-15 (PN G 6.8+4.1)

This PN surrounds a [WC 4-6] star. The integrated spectrum was presented in Gesicki & Acker (1996). From our observations we estimate the diameter as 6″, assume a broadened slit width of 0.75 of the PN diameter and the pixels along the slit are centred on 0.2 and 0.8 times $R/R_{\rm out}$. The long-slit analysis is shown in Fig. 4. This model does not change the parameters presented in Gesicki & Acker (1996): the expansion velocity is constant with radius at a value of 16 km/s, and a turbulent broadening with a comparable value of 15 km/s has to be introduced. Any attempt to introduce a velocity gradient yields worse fit to the lines. This is the least spatially resolved PN from our sample and the discovered large turbulent motions smear out any detail in its structure.

4.4. Nebula M 1-40 (PN G 8.3-1.1)

This is the nearest of the four PN analyzed in this paper and the one spatially most resolved. Górny & Stasinska (1995) classify it as irregular. The long-slit spectrum indicates bipolarity, which is not visible in integrated spectra. Its manifestation is clearly seen in in the [N II] line (see Fig. 5, right panel, second from the top), where the open and filled symbols correspond to line shapes taken on opposite sides of the nebular centre. On one side of the nebula the intensity is higher at negative velocities (filled triangles and squares), while on the other side (open symbols) the receding velocities have stronger emission. We cannot distinguish between different morphological types as presented in

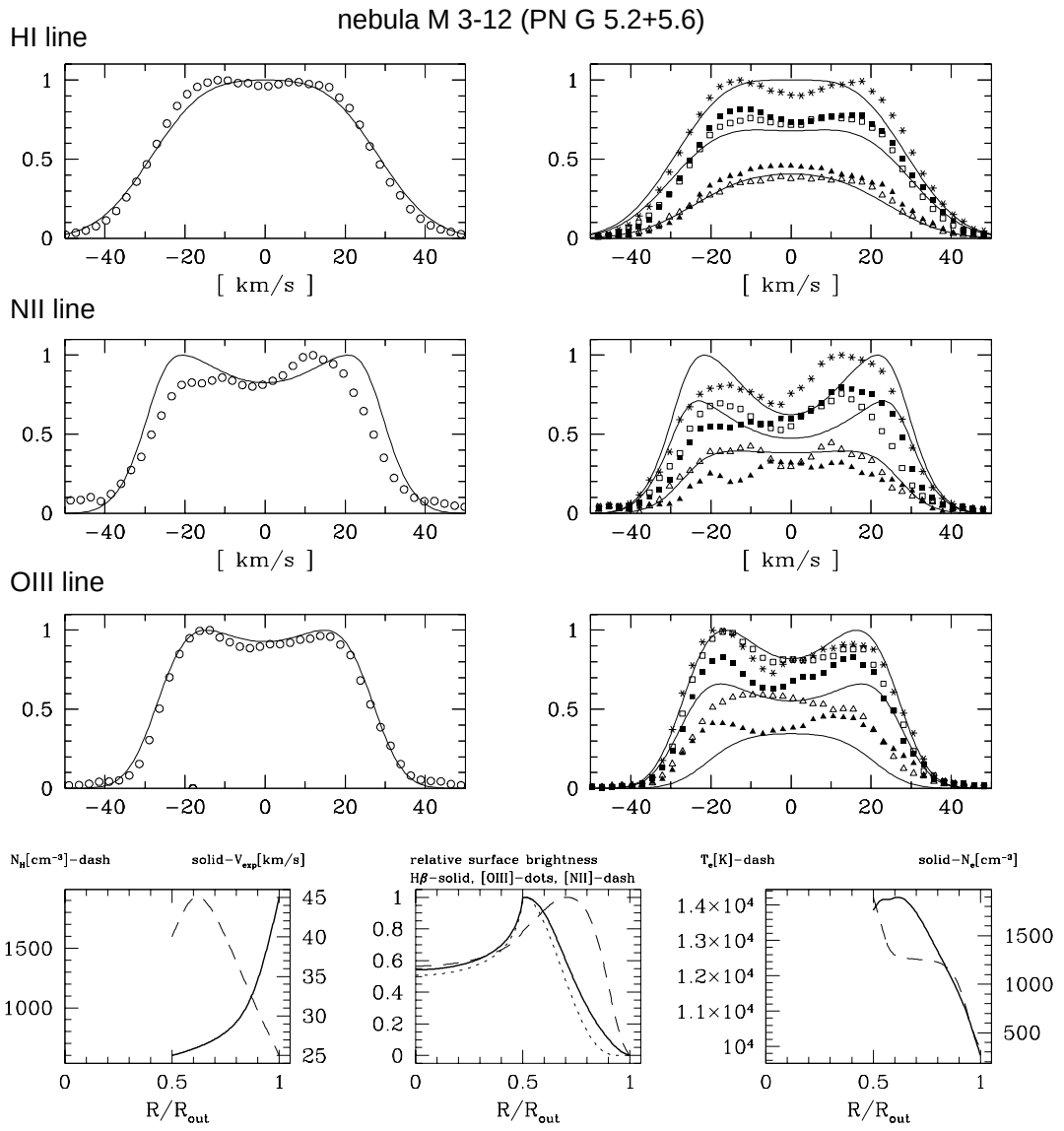

Fig. 2. The results for the PN M 3-12 (PN G 5.2+5.6). Each row of two panels presents the calculated (solid line) and the observed (symbols) line profiles. The observed Hα profile is compared with the calculated Hβ (upper row). The following rows show [N II] 6584 Å (middle row) and [O III] 5007 Å. In each row the left panel represents the integrated spectrum over the long slit, while the right panel gives a sequence of spectra along the slit. Stars mark the line observed in the very center of PN, squares at some distance from the center, triangles at the outer edge. The filled symbols correspond to one side of the slit, open symbols to the opposite side. The assumptions leading to calculated profiles (solid lines) are described in the text. In the lowest row we present the model structure. The lower left panel presents the assumed velocity and density distribution in the shell. The density is the hydrogen number density. The surface brightness distribution (lower middle panel) and the calculated electron temperature and density (lower right panel) are also shown.

Corradi & Schwarz (1995), whether the PN is axially or point symmetric, or if there are two or more lobes present. The slit orientation is also unknown. We can only conclude that the velocity field includes a component which shows a monotonic velocity gradient along the slit. The effect for M 1-40 is not as strong as for two PN presented later in the discussion (the 'bipolar' component is not as dominant) and we decided to still apply our spherically symmetric modeling.

We assumed the width of the seeing-broadened slit to be 0.75 of the PN diameter (the pixels along the slit are centered on 0.3 and 0.8 times $R/R_{\rm out}$). The density structure has been adopted to agree with monochromatic images published by Schwarz et al. (1992); the original images were kindly provided to us by the authors. In the [O III] image the inner, quasi-circular rim is clearly resolved, with the diameter (peak to peak) of 2″ (Corradi, 1997). In our calculations, by putting the peak density close to the inner boundary, the diameter comes out as 2.3″. The brightness fall-off is also similar to what is observed. The Hα+[N II] image has much poorer seeing, not allowing us to resolve the inner rim.

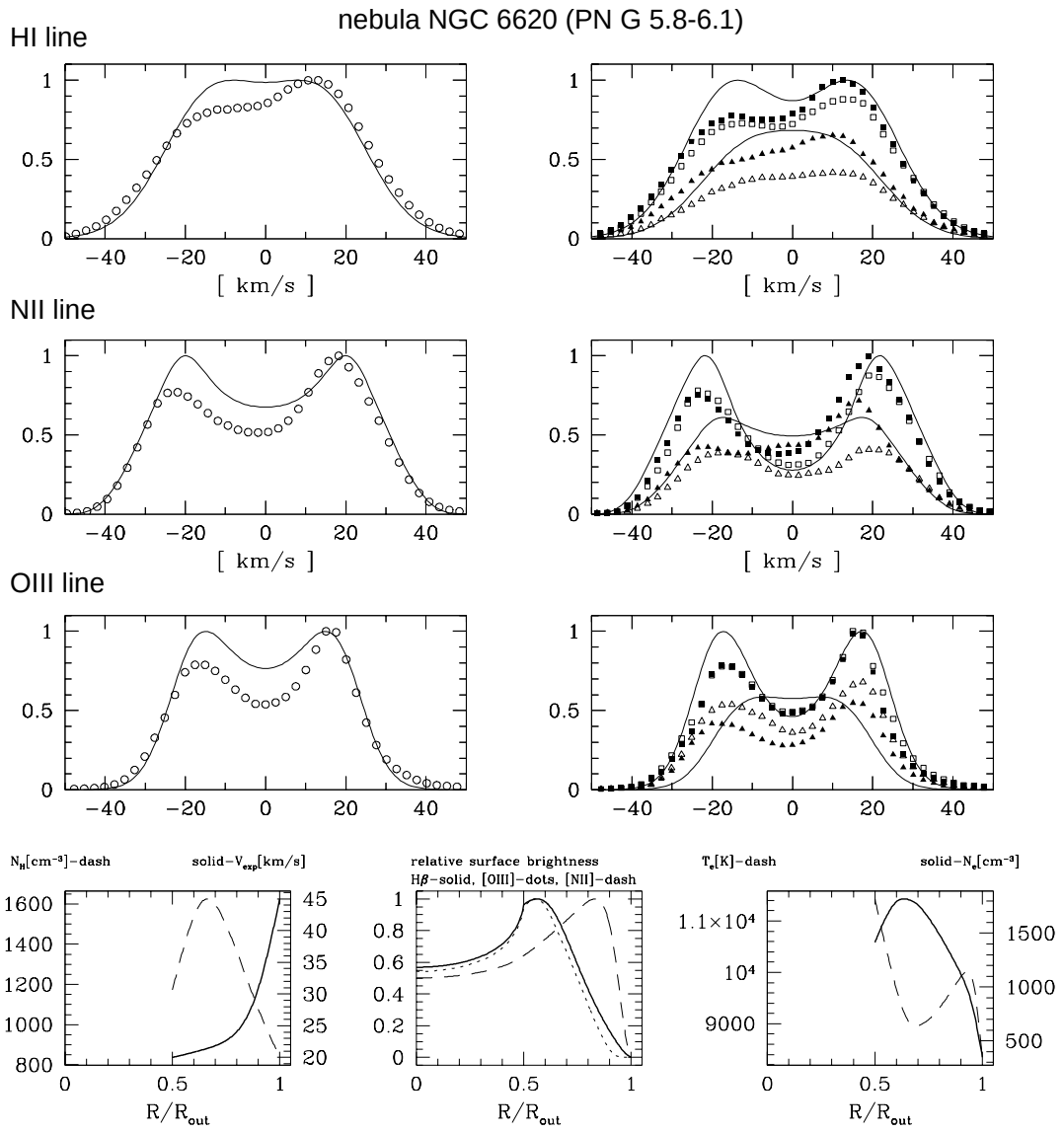

Fig. 3. The results for the PN NGC 6620 (PN G 5.8-6.1). Setup and symbols are explained in the caption to Fig. 2 with the difference in the right panels that we have no spectrum centred at the PN: the squares mark two adjacent spectra centred on either side of the slit.

The images of Schwarz et al. (1992) and our spectra both show that the [O III] line forms in a more condensed region than Hα. However, in our model the regions differ only slightly (see the panel showing the surface brightness). The details of the line shapes are also not well fitted, as seen from Fig. 5. We have tried a range of nebular sizes, and different density and velocity fields but reached the conclusion that the situation cannot be improved within a simple nebular structure. The emission wings present in the [O III] lines are interpreted by Schönberner et al. (1997) in terms of an expanding outer density wave. However, such a structure should be even more pronounced in the [N II] lines (compare the relatively well fitted [N II] lines in Fig. 5). Aspherical morphology can be the cause of this discrepancy. We did not attempt more elaborate models.

5. Discussions and conclusions

Although more observational material is available on additional nebulae, we selected the present four objects because for each of them three strong emission lines are observed which are each spatially resolved. The O III ion emitting at 5007Å is present in the inner nebular region which is more highly ionized by the central star, while the N II ion emitting at 6584Å is present in the outer nebular layers, close to the hydrogen ionization boundary. The hydrogen Hα line forms through the entire PN and is mostly severely thermally broadened. These three emission lines together constitute a good set of nebular probes, covering the range of condition encountered in most PN. Our computer codes allow for modeling other lines, but the three lines are the strongest ones and the easiest to observe. They can be taken as the standard testing lines for the nebular structure. Deducing

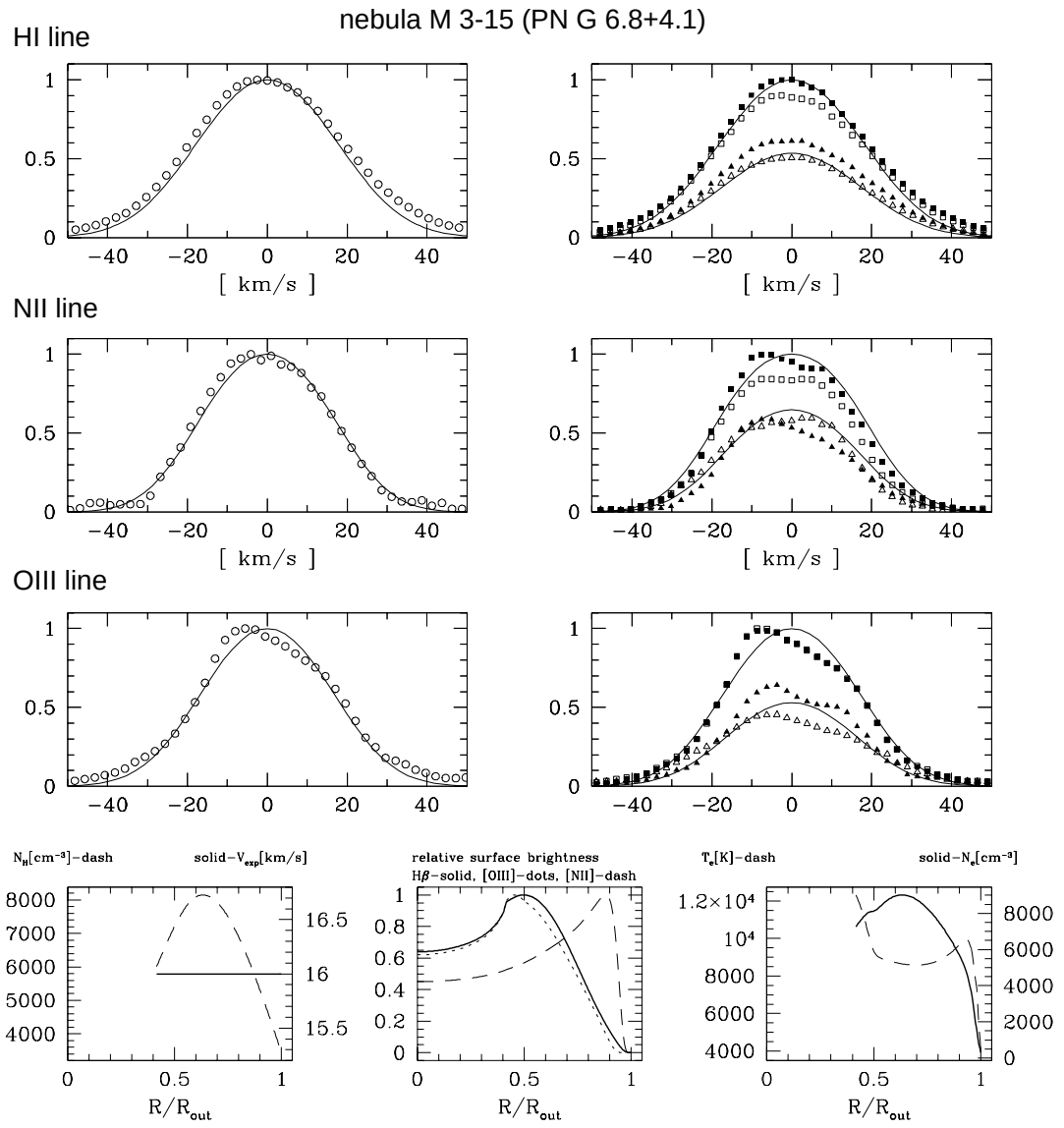

Fig. 4. The results for the PN M 3-15 (PN G 6.8+4.1). Setup and symbols are explained in the caption to Fig. 2 and Fig. 3.

the nebular structure from a long-slit analysis of [O III] only, although possible, is not reliable.

Two nebulae which we observed but could not model for the present paper can serve as a good illustration of the value of the long-slit analysis. Both nebulae are found to have a pronounced bipolar structure (stronger than for discussed earlier M 1-40) and an analysis based on aperture spectra and the assumption of spherical symmetry would be misleading:

– NGC 5873 (PN G 331.3+16.8); shows symmetric [O III] long-slit spectra but reveals a clear bipolar structure on long-slit spectra in Hα and [N II]. This is illustrated in Fig. 6, where the triangles mark the spectra at some distance from the centre of the PN: at one side almost all matter is approaching us with velocity of about 15 km s^{-1} while the opposite side is receding with a similar velocity. For this object we see some evidence for such structures in the images published in Schwarz et al. (1992), where the Hα image shows knots which do not form a ring.
– Although symmetric when imaged (Schwarz et al. 1992) or on (aperture) spectra, Me 2-1 (PN G 342.1+27.5) shows a pronounced bipolar structure in long-slit spectra (see Fig. 7). The hydrogen lines are symmetric, but the [N II] lines (compare the triangles which mark the spectra away from the centre) show that on one side almost all matter is approaching us with a velocity $\sim$ 40 km s^{-1} while on the opposite side the nebula is receding with a similar velocity.

The model radial density distributions are limited mainly by the spatial resolution of the observations. For our four PN we can estimate the location of the maximum density (assuming an inverse parabola function) and the density contrast between the maximum and the nebular edges. The [N II] observations pose some constraint on how the density declines towards the outer

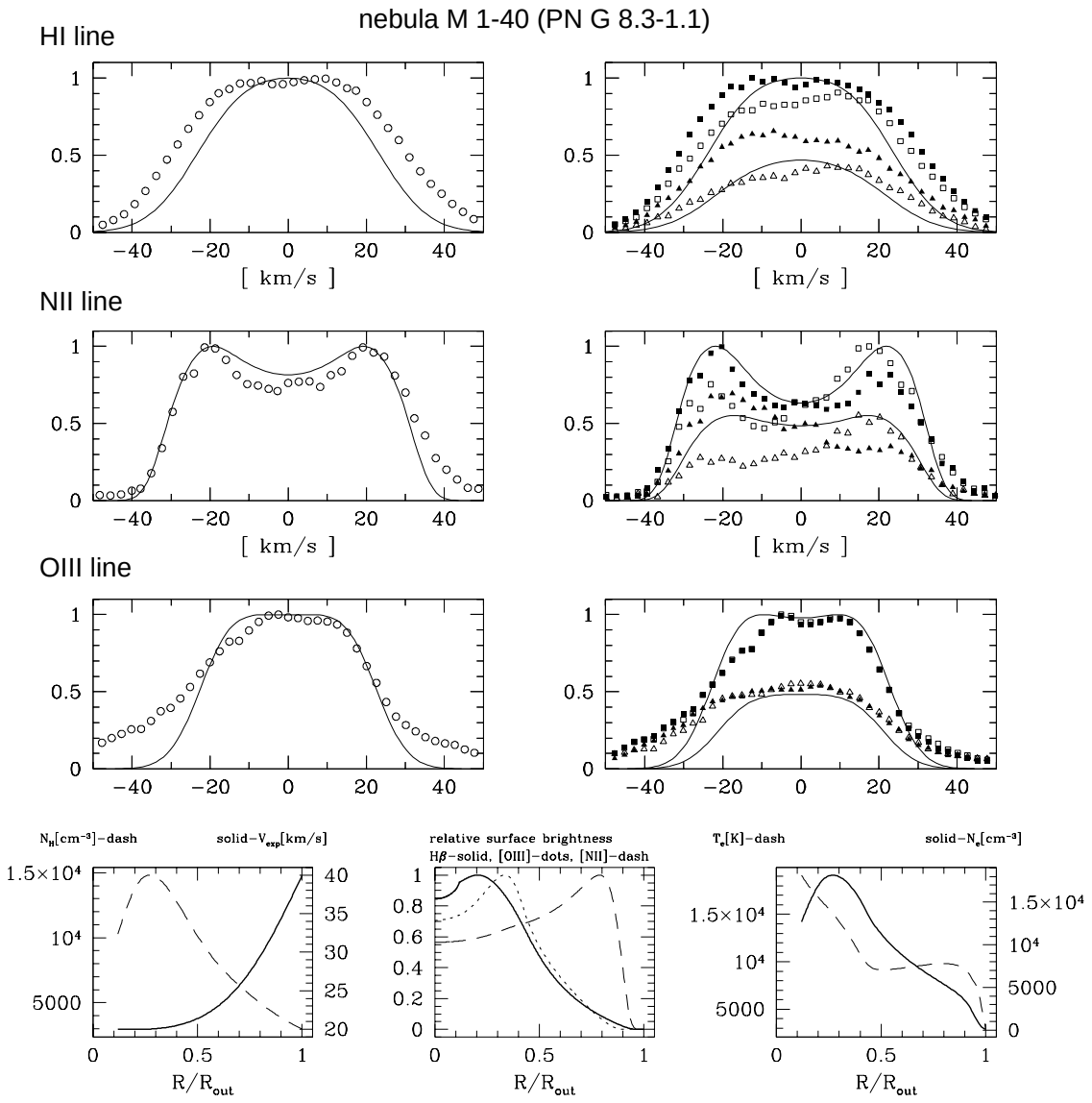

Fig. 5. The results for the PN M 1-40 (PN G 8.3-1.1). Setup and symbols are explained in the caption to Fig. 2 and Fig. 3.

nebular edge. Further constraints cannot be deduced from the present data.

Instead of fitting a single value for the expansion velocity, we deduce the velocity field by fitting all observed spectral lines. The assumed density distribution is required for this step. Except for M 3-15, we find that a linear dependency cannot explain the observed profiles. The derived velocity fields significantly improve the fit. The overall velocity fields are still not fully determined, but changing the velocity by $5\,\mathrm{km\,s^{-1}}$ in a place where one of the lines form, even if it improves the fit of this line, significantly worsens the other two. For the low-intensity line wings the accuracy is less.

The resulting velocity field is used to calculate the parameter V_{av}, which is the radially averaged expansion velocity weighed by the density distribution. This parameter better represents the expansion velocity of a PN than the observed double peak separation or the FWHM of the observed emission lines (Weinberger 1989). The value takes into consideration that the velocity can vary significantly over the nebula. Using only the [O III] line, which may come from only the inner part of the nebula, may give a biased result.

Including three PN from our Paper I (IC 418 (PN G 215.2-24.2), IC 2165 (PN G 221.3-12.3) and IC 3568 (PN G 123.6+34.5)), we have a sample of seven objects with established velocity fields. We find that in five of the seven, the expansion velocity slowly increases in the inner nebular layers and steeply increases in the outer layers. Such a velocity law is required to explain the narrower [O III] lines, broader [N II] lines, splitting of the central profiles and high velocity wings. The two exceptions are M 3-15 and IC 3568.

Mellema (1994), analyzing the kinematics of his spherically symmetric nebular models, predicts that the velocities increase

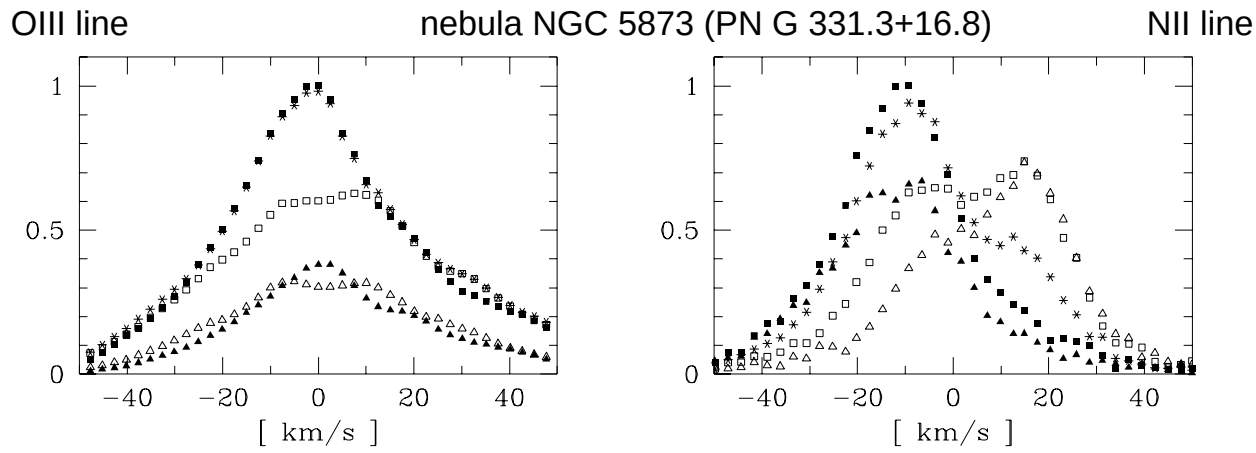

Fig. 6. The long-slit spectra of the PN NGC 5873 (PN G 331.3+16.8). As in the preceding figures the inner spectra are marked with squares, the outer with triangles; open and filled symbols correspond to either side of the PN along the slit. The spectrum corresponding to the very center is marked with stars.

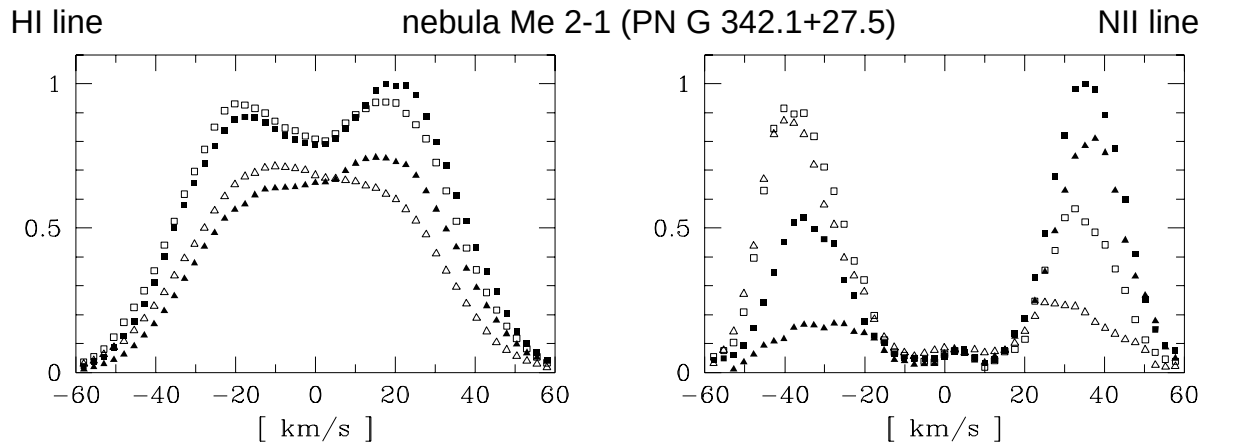

Fig. 7. The long-slit spectra of the PN Me 2-1 (PN G 342.1+27.5). The meaning of symbols is the same as in Fig. 6 except the stars are not present.

outwards. Similar velocity fields are also obtained by Frank (1994) for model nebulae in the so-called hydrogen-ionization phase, when the PN is fully ionized. We note that, in contrast to these two papers, in our models an ionization front appears to be commonly present: among our seven objects there is one exception, IC 3568 which is discussed below. Except for the prediction regarding the ionization front, our findings agree well with the predictions of the hydro-dynamical models.

The two cases where the velocity does not appear to increase at larger radii are:

– M 3-15 is an object with [WC] type central star. We can confirm the conclusion from Gesicki & Acker (1996) that the equal width of the three observed lines can be best explained in terms of turbulence, affecting the different emitting ions to the same degree. The turbulence is so high value that the details in the velocity field cannot be determined from our data. It is possible that nebulae with [WC] central stars have less regular velocity fields than the other PN discussed here. The assumed very high turbulence may only be an approximation to a more complicated situation with strong velocity variations in radial direction.
– IC 3568, taken from Paper I is the only density-bounded PN in our sample. Its velocity field reaches a terminal value, making it different from the velocity fields found for the five ionization-bounded PN. It is also characterized by the presence of a low-density halo (Harrington & Feibelman, 1983).

We are aware of the limitations of our method. The assumed spherical symmetry and sharp edges may be an important difference between our models and real nebulae. Nevertheless the simultaneous presence of ionization front and the acceleration in the outer layers is found for five nebulae. The sixth case, a density-bounded nebula, shows no evidence for acceleration in the outer layers. The two features are deduced separately: the presence of the ionization front follows from the photoionization modeling and fitting the line ratios, whilst the velocity field

follows from modeling the details of the line shapes. Our finding that the presence of outward acceleration of the PN is related to the ionization front, is in agreement with Mellema (1994) who writes: "because of the action of the ionization front the outer parts of the envelope have acquired a large velocity". It seems that we indeed observe such an interaction.

The conclusion of Mellema concerns one specific evolutionary phase in his models. Is it possible that our five PN are just in this phase? This could be due to our selection criterium: the absence of obvious asphericity in the nebulae. The presence of an ionization front indicates that the nebula is sufficiently dense to contain the ionizing radiation of the star. How long this phase lasts depends on the expansion of the nebula and on its mass. If the nebula expands slowly while the star evolves fast, one can expect hot central stars while otherwise the objects will primarily have cooler central stars. Some of the central stars for our sample have very high effective temperature, which indicates an advanced evolutionary phase. So it is possible that we have mostly selected higher-mass PN: this can be related to the fact that only the intrinsically brighter PN towards the Bulge were observed (Zijlstra et al. 1997). However, it is also possible that asphericities become more pronounced after the passage of the ionization front through the whole nebula: the PN fragments, loses sphericity and symmetry in line profiles, and we reject it from our sample. A larger sample extending to fainter nebulae would be desirable to continue this investigation.

Acknowledgements. The authors wish to thank Dr. R.Corradi for providing the original files with published images of M 1-40, NGC 5873 and Me 2-1. This project was partially supported by the PICS/JUMELAGE "Astronomie Pologne" programme. One of the authors (K.G.) thanks ESO for a two-month visitorship in 1995, which allowed him to start the presented work and to perform a significant part of it. K.G. and R.Sz. acknowledge partial support from KBN grants No. 2.P03D.026.09 and 2.P03D.027.10.

References

Acker A., Köppen J., Stenholm B., Jasniewicz G., 1989, A&AS 80, 201
Acker A., Köppen J., Stenholm B., Raytchev B., 1991, A&AS, 89, 237
Acker, A., Ochsenbein, F., Stenholm, B., et al., 1992, Strasbourg - ESO Catalogue of Galactic Planetary Nebulae. ESO, Garching (CGPN)
Aller L. H., Keyes C. D., 1987, ApJS, 65, 405
Bedding T.R., Zijlstra A.A., 1994, A&A, 293, 955
Chu Y.-H., Manchado A., Jacoby G.H., Kwitter K.B., 1991, ApJ 376, 150
Corradi R. L. M., Schwarz H. E., 1995, A&A 293, 871
Corradi R. L. M., 1997, private communication
Frank A., 1994, AJ 107, 261
Frank A., Balick B., Icke V., Mellema G., 1993, ApJ, 404, L25
Gesicki K., Acker A., Szczerba R., 1996, A&A, 309, 907 (Paper I)
Gesicki K., Acker A., 1996, Ap&SS, 238, 101
Górny S.K., Stasinska G., 1995, A&A, 303, 893
Harrington J. P., Feibelman W. A., 1983, ApJ 265, 258
Marten H., Schönberner D., 1991, A&A 248, 590
Mellema G., 1994, A&A 290, 915
Pottasch S.R., 1984, "Planetary Nebulae", ASSL vol.107, D.Reidel Dordrecht/Boston/Lancaster
Preite-Martinez A., Acker A., Köppen J., Stenholm B., 1989, A&AS, 81, 309
Sabbadin F., Gratton R.G., Bianchini A., Ortolani S., 1984, A&A 136, 181
Sabbadin F., Strafella F., Bianchini A., 1986, A&AS 65, 259
Samland M., Köppen J., Acker A., Stenholm B., 1992, A&A, 264, 184
Schönberner D., Steffen M., Stahlberg J., Kifonidis K., Blöcker T., 1997, to appear in: Advances in Stellar Evolution, eds. R.Rood, A.Renzini, Cambridge U. Press
Schwarz H. E., Corradi R. L. M.,Melnick J., 1992, A&AS, 96, 23
Spyromilio J., 1995, MNRAS, 277, L59
Tylenda R., Acker A., Stenholm B., Köppen J., 1992, A&AS, 95, 337
Van de Steene G.C., Zijlstra A.A., 1994, A&AS, 108, 485
Weinberger R., 1989, A&AS, 78, 301
Wilson O.C., 1950, ApJ 111, 279
Zijlstra A.A., Acker A., Walsh J.R., 1997, A&AS, in press
Zhang C.Y., Kwok S., 1993, ApJS, 88, 137

This article was processed by the author using Springer-Verlag LaTeX A&A style file *L-AA* version 3.